Oxidation of Metals, Vol. 30, Nos. 5/6, 1988

Effect of 0.1 at.% Zirconium on the Cyclic Oxidation Resistance of β-NiAl

Charles A. Barrett*

Received March 17, 1988; revised June 1, 1988

The effect of 0.1 at.% Zr (0.2 wt.% Zr) on the cyclic oxidation of hipped β-NiAl was studied. Oxidation testing was performed in static air at 1100–1200°C, using 1-hr exposure cycles for test times up to 3000 hr. The weight change versus time data were modeled with the COSP computer program to analyze and predict cyclic-oxidation behavior. Zr additions significantly change the nature of the scale-spalling process during cooling so that the oxide spalls near the oxide–air interface at a relatively low depth within the scale. Without Zr, the predominantly α-Al_2O_3 scale tends to spall randomly to bare metal at relatively high effective-scale-loss rates, particularly at 1150°C and 1200°C. This leads to higher rates of Al consumption for the Zr-free aluminide and much earlier depletion of Al, leading to eventual breakaway (i.e., failure).

KEY WORDS: cyclic oxidation; β-nickel aluminide; zirconium effect; scale spalling; computer modeling.

INTRODUCTION

β-NiAl has long been an attractive oxidation-resistant coating material for nickel-base superalloys. For temperatures approaching 1200°C, the aluminide provides a high degree of oxidation resistance due to the continuous formation of protective Al_2O_3.

During the past 15–20 years, a number of investigations have been carried out here at NASA Lewis Research Center exploring primarily the cyclic oxidation and hot-corrosion resistance of β-NiAl both as a coating for superalloys as well as a bulk alloy.[1-6] Parallel work here at NASA Lewis

*National Aeronautics and Space Administration, Lewis Research Center, Cleveland, Ohio 44135.

0030-770X/88/1200-0361$06.00/0

has also focused on the oxidation resistance of MCrAl alloys containing dispersed oxides such as ThO_2 or Y_2O_3. Investigations of alloy additions to the MCrAl centered mainly on Zr, which greatly improved the spall resistance of scales formed on such alloys in high-temperature cyclic oxidation at an optimum Zr composition of near 0.2 wt.%.[7-9]

For this reason, a similar amount of Zr was alloyed to a bulk cast β-NiAl and tested in long-time cyclic-oxidation exposures for times out to 3000 hr at 1200°C. This alloy had excellent oxidation resistance but was extremely brittle due to Zr segregation to the grain boundaries. Alloys both with and without Zr were then prepared by a powder metallurgy, high-pressure/high-temperature process (i.e., PM/Hipping) process and were tested under the same conditions as well as at 1150 and 1100°C. These alloys were much less brittle than were comparable cast alloys. The kinetics of the oxidation and spalling process for these PM/Hipped alloys were evaluated in terms of specific weight charge versus time data and form the basis for this report. The resulting oxide phases were determined by X-ray diffraction (XRD) analysis. Additional postrun tests were also performed.

PROCEDURES

The three β-NiAl alloy powder compositions studied were obtained from Alloy Metals, Inc., of Troy, Michigan, two of which contained ~0.2 wt.% Zr. The alloy powders were placed in 4-in. × 3/4-inch-diameter stainless-steel tube capsules and hipped at 1288°C (2350°F) and 20,000 lb. for 2 hr. The resulting rod was trimmed and machined into small disk coupons with a ground 32 rms finish and a small hole drilled for hanging during cyclic-oxidation testing. Table I summarizes the chemistry of the three alloys tested. The three PM/Hipped alloys were denoted as alloys 1, 2, and 3, as indicated in Table I. Alloy 1 contains no Zr, while alloy 3 has a significantly lower Al level just within the single-phase β-NiAl region at 800°C. Alloys 1 and 2 were essentially stoichiometric β-NiAl.

These three alloys were tested in cyclic oxidation at 1200, 1150, and 1100°C for up to 3000 1-hr cycles in order to determine the variation in behavior. The alloys were examined at selected intervals using XRD to determine the oxide phases that formed within the scale. Post-test SEM and microprobe analyses were also performed on selected samples.

RESULTS AND DISCUSSION

Gravimetric

The specific weight change versus time data are listed in Table II. In order to analyze the data kinetically, they were divided into two groups.

Table I. Composition and History of β-Nickel Aluminide Alloys Tested

	β-nickel aluminides
Alloy[a]	Composition
1	Ni-46.57 at.% Al-0.0 at.% Zr (28.6 wt.% Al-0.0 wt.% Zr)
2	Ni-48.28 at.% Al-0.09 at.% Zr (30.0 wt.% Al-0.19 wt.% Zr)
3	Ni-38.05 at.% Al-0.10 at.% Zr (22.0 wt.% Al-0.19 wt.% Zr)

[a] Alloy powders were placed in 4 by 3/4 in. diameter stainless steel tube capsules hipped at 2350°F at 20,000 lb for 2 hr. Rod trimmed and machined into disk coupons with small hanger hole. With a machine ground 32 rms finish.

First, the specific weight change versus time data for the first 100 hr was fitted by linear regression to

$$\Delta W/A = k_p^{1/2} t^{1/2} \tag{1}$$

to derive the parabolic rate constant, k_p.*

Figure 1a shows the specific weight change versus time plot at 1200°C for the three alloys along with their Al and Zr contents. Weight-change valves for the Zr-free alloy drop steadily with time as the alloy spalls continuously with each cycle. The alloy samples appear at any given time during the 3000-hr test to be metallic (i.e., nearly bare of scale). The Zr-containing, stoichiometric alloy 2 maintains a thin, tightly-adherent, dark-gray scale with negligible spall. Alloy 3 behaves similarily but has a lighter-gray scale. At 1150°C, the same trends are present but are not so extreme (Fig. 1b). The Zr-containing alloys 2 and 3 still maintain their thin, tightly adherent, dark or light-gray scale throughout the test with minimal spalling. Figure 1c shows the three alloys tested at 1100°C for 3000 1-hr cycles. Again, the Zr-containing alloys appear superior, but the differences between the Zr-free and Zr-containing alloys are not nearly so extreme.

The specific weight-change/time data were divided into two time groupings for analysis. The first 100 hr of data were used to derive k_p as in Eq. (1). For alloys 2 and 3, this is possible because the spalling fractions are so low that within experimental accuracy even at 1200°C the curves are

*All k_p values used or referenced in this report are in terms of $(mg/cm^2)^2/hr$.

Table II. Specific Weight Change/Time Data for the Individual β-Nickel Aluminide Alloy Samples Tested in Cyclic Oxidation (mg/cm^2)

	Hipped Ni-48.3Al-.1Zr					Hipped Ni-38.1Al-.1Zr				Hipped Ni-46.6Al			
	1200°C		1150°C	1100°C		1200°C	1150°C	1100°C		1200°C	1150°C	1100°C	
Time, hours	625-6	660-4	672-5	673-3	673-6	660-2	672-1	673-1	673-2	660-3	672-4	673-4	673-5
1	0.17	0.14	0.03	0.14	0.00	0.08	0.08	0.14	0.03	0.20	−0.03	−0.06	0.03
15	0.59	0.42	0.39	0.17	0.17	0.48	0.48	0.34	0.25	0.00	0.50	0.11	0.17
30	0.73	0.56	0.42	0.06	0.11	0.78	0.64	0.31	0.20	−0.73	0.50	0.00	0.11
45	0.78	0.73	0.59	0.22	0.22	1.01	0.87	0.42	0.31	−1.71	0.53	0.14	0.22
60	0.95	0.87	0.62	0.45	0.48	1.09	0.92	0.67	0.56	−2.74	0.53	0.34	0.42
75	1.15	0.98	0.53	0.36	0.42	1.23	0.98	0.62	0.50	−3.97	0.25	0.25	0.36
90	1.12	1.06	0.87	0.31	0.39	1.34	1.12	0.62	0.45	−5.09	0.42	0.20	0.11
100	1.15	1.31	0.84	0.53	0.62	1.57	1.15	0.78	0.70	−5.87	0.31	0.45	0.53
115	1.17	1.26	0.92	0.34	0.45	1.57	1.26	0.64	0.50	−6.79	−0.08	0.22	0.31
130	1.26	1.34	0.95	0.47	0.48	1.62	1.37	0.76	0.61	−8.02	−0.17	0.34	0.36
145	1.29	1.34	0.95	0.56	0.56	1.73	1.43	0.78	0.67	−9.31	−0.25	0.45	0.36
160	1.29	1.40	1.06	0.67	0.62	1.79	1.48	0.81	0.73	−10.54	−0.25	0.47	0.45
175	1.34	1.37	0.90	0.59	0.62	1.85	1.51	0.84	0.73	−11.91	−0.50	0.42	0.42
190	1.40	1.43	1.06	0.61	0.62	1.90	1.62	0.84	0.75	−13.22	−0.42	0.36	0.42
200	1.48	1.62	1.09	0.75	0.73	2.01	1.68	0.95	0.87	−14.06	−0.48	0.50	0.53
250	1.79	1.82	1.20	0.67	0.73	2.24	1.93	0.95	0.87	−18.56	−0.62	0.50	0.48
300	1.93	1.79	1.29	0.75	0.73	2.21	2.10	1.12	0.95	−23.45	−0.76	0.39	0.36
350	2.10	2.04	1.40	0.81	0.81	2.24	2.24	1.20	1.09	−28.62	−0.98	0.45	0.42
400	1.79	2.04	1.48	0.95	0.98	2.13	2.41	1.34	1.26	−34.13	−1.32	0.34	0.34
450	1.79	2.15	1.54	0.89	0.90	2.04	2.57	1.40	1.26	−39.86	−1.74	0.17	0.22
500	1.96	2.27	1.57	1.20	1.09	2.01	2.69	1.60	1.40	−45.00	−2.24	0.11	0.17
550	2.04	—	1.59	1.17	1.15	—	2.94	1.71	1.45	—	−2.77	0.00	0.03
600	1.99	—	1.71	1.23	1.18	—	2.88	1.76	1.56	—	−3.44	0.00	0.03
650	1.90	—	1.76	1.12	1.09	—	2.99	1.73	1.51	—	−4.03	−0.06	−0.08
700	1.90	—	1.82	1.28	1.29	—	3.11	1.90	1.68	—	−4.82	−0.03	0.06
750	1.93	—	1.82	1.31	1.26	—	3.19	2.04	1.76	—	−5.66	−0.06	0.00
800	1.87	—	1.93	1.28	1.20	—	3.27	2.01	1.79	—	−6.41	−0.22	−0.14
850	1.79	—	1.99	1.37	1.26	—	3.36	2.15	1.90	—	−7.31	−0.28	−0.14
900	1.82	—	2.01	1.40	1.26	—	3.41	2.21	1.96	—	−8.20	−0.47	−0.22
950	1.87	—	2.07	1.51	1.34	—	3.50	2.35	2.12	—	−9.04	−0.53	−0.22
1000	1.71	—	2.18	1.51	1.29	—	3.55	2.41	2.15	—	−9.94	−0.64	−0.39
1100	—	—	2.18	1.62	1.46	—	3.72	2.57	2.35	—	−10.92	−0.67	−0.36
1200	—	—	2.27	1.56	1.43	—	3.83	2.66	2.40	—	−11.87	−0.78	−0.45
1300	—	—	2.29	1.59	1.48	—	3.92	2.77	2.51	—	−12.85	−0.81	−0.50
1400	—	—	2.46	1.62	1.54	—	4.09	2.88	2.63	—	−14.22	−0.61	−0.59
1500	—	—	2.49	1.68	1.57	—	4.20	3.05	2.79	—	−15.40	−0.87	−0.64
1600	—	—	2.55	1.65	1.60	—	4.14	3.13	2.85	—	−16.04	−1.15	−0.87
1700	—	—	2.55	1.68	1.62	—	4.20	3.25	2.96	—	−17.22	−1.20	−0.95
1800	—	—	2.71	1.68	1.65	—	4.31	3.33	3.05	—	−18.84	−1.26	−1.04
1900	—	—	2.69	1.76	1.76	—	4.34	3.44	3.21	—	−20.16	−1.28	−1.07
2000	—	—	2.77	1.73	1.74	—	4.42	3.50	3.27	—	−21.75	−1.40	−1.23
2100	—	—	2.74	1.79	1.82	—	4.34	3.55	3.35	—	−23.35	−1.59	−1.40
2200	—	—	2.91	1.79	1.88	—	4.45	3.64	3.44	—	−25.37	−1.62	−1.46
2300	—	—	2.85	1.73	1.82	—	4.48	3.67	3.44	—	−26.91	−1.76	−1.60
2400	—	—	3.02	1.82	1.93	—	4.56	3.75	3.58	—	−28.92	−1.79	−1.74
2500	—	—	3.08	1.82	1.93	—	4.59	3.81	3.63	—	−30.66	−1.93	−1.91
2600	—	—	3.10	1.87	1.99	—	4.42	3.81	3.66	—	−33.29	−2.82	−2.24
2700	—	—	3.10	1.84	1.93	—	4.39	3.81	3.66	—	−35.98	−2.96	−2.44
2800	—	—	3.16	1.95	1.82	—	4.42	3.92	3.80	—	−38.67	−2.99	−2.49
2900	—	—	3.08	1.98	2.07	—	4.39	3.95	3.80	—	−41.58	−3.13	−2.63
3000	—	—	3.10	1.93	1.99	—	4.39	3.95	3.80	—	−44.68	−3.32	−2.89

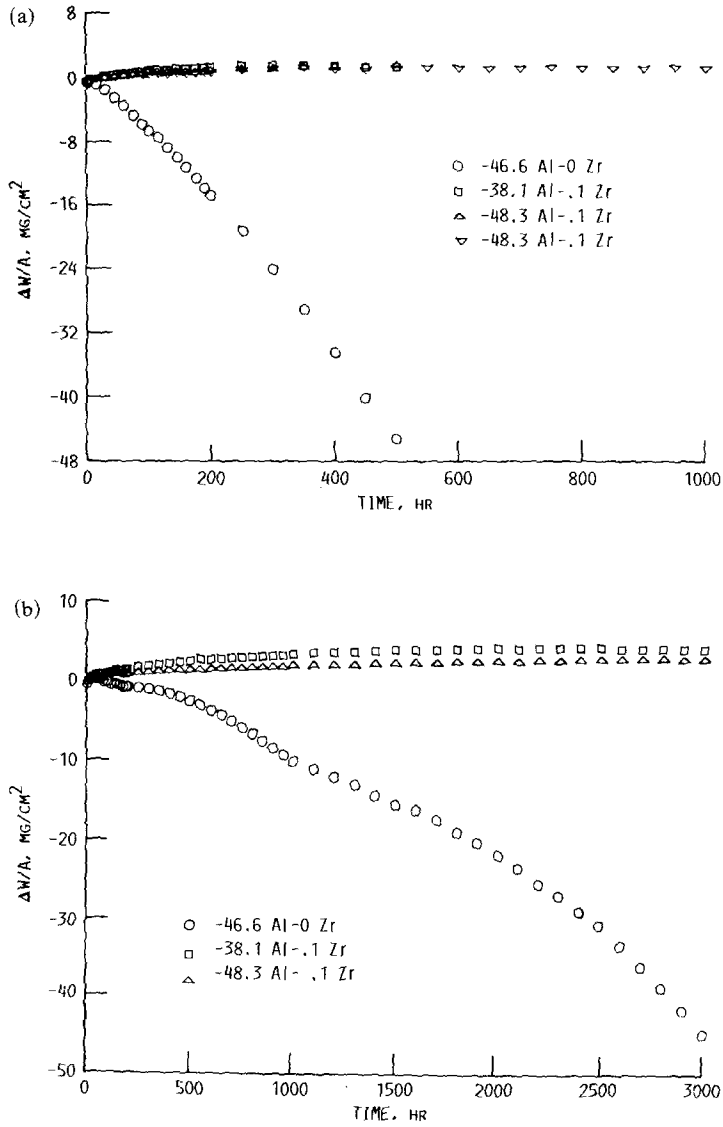

Fig. 1. Specific weight-change-time data for three β-nickel aluminide alloys tested at three temperatures for 1-hr exposure cycles in static air at (a) 1200°C, (b) 1150°C, and (c) 1100°C.

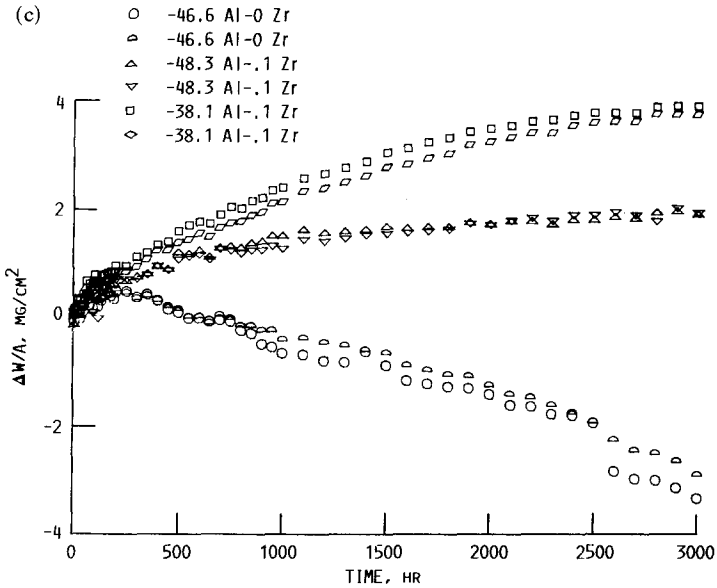

Fig. 1. Continued.

effectively parabolic at least for the first few hundred hours. Selected samples were checked isothermally to verify this approach. For the Zr-free alloy 1, however, at both 1200 and 1150°C, the specific weight-change data were negative very early. Therefore, k_p values could not be derived even at early times in a cyclic run. For this reason, k_p values were derived from 24-hr isothermal testing based on continuous weighing with a special Cahn microbalance system.[10]

POST-TEST ANALYSIS

X-Ray Diffraction Results

X-ray diffraction analyses of the sample surfaces and any collected spall are summarized in Table III after various times and at the end of the tests for all three alloy samples. In general, the Zr-containing alloys form mainly α-Al_2O_3 and in most cases significant amounts of ZrO_2 and $NiAl_2O_4$ on their surfaces. The spall contains α-Al_2O_3, a little ZrO_2, and in some cases a small amount of $NiAl_2O_4$ and NiO. In all but one case, the Zr-free alloy formed α-Al_2O_3 as a surface scale. An interesting aspect observed while collecting the spall of the Zr-free alloy was that in the 1150°C test, significant spall was not observed in the collector cup until the interval

Table III. Summary of X-Ray Diffraction Results of β-Nickel Aluminide Samples for Surface Oxide Phases after Various Exposure Times in Cyclic Oxidation[a]

Alloy, at.%	Run no.	Temperature, °C	X-ray diffraction surface phases at various times, hours[b]									Spall, when observed
			1	100	200	500	1000	1500	2000	2500	3000	
Ni-48.3Al-.1Zr	625-6	1200	A	A	A, Z	A, S, Z	A, S, Z	—	—	—	—	100-A 500-N, S, A 200-A, N, S 1000-A, N, S
	660-4	—	A	A	A, Z	A, Z	—	—	—	—	—	200-A, N 500-A, N, S
	672-5	1150	A	A, S	A, S, Z	A	A	A, S, Z	—	A, Z, S	A, Z, S	3000-A
	673-3	1100	A	A, Z	A, Z	A, Z, S	A, Z	A, S, Z	A, S, Z	A, S, Z	A, Z, S	
	673-6	1100	A	A, Z	A, Z	A, Z	A, S, Z	A, S, Z	A, S, Z	A, S, Z	A, Z, S	
Ni-38.1Al-.1Zr	660-2	1200	A	A	A, Z	A, S, Z	—	—	—	—	—	100-A, N, S 500-N, S, A 200-A, N, S
	672-1	1150	A	A	A, S, Z	A	A, Z, S	A, S, Z	—	A, Z, S	A, Z	500-A, S, N, Z 3000-A 1500-A, N, S
	673-1	1100	A	A, S, Z	A, Z	A, Z, S	A, S, Z	A, S, Z	A, S, Z	A, S, Z	A, Z, S	
	673-2	1100	A	A, S, Z	A, Z, S	A, Z, S	A, S, Z	A, S, Z	A, S, Z	A, S, Z	A, Z, S	
Ni-46.6Al	660-3	1200	A	A	A	A	—	—	—	—	—	100-A, S 500-N, A, S 200-A, N, S
	672-4	1150	A	A	A	A	A	A	—	A	A	3000-A
	673-4	1100	A	A	A	A	A	A	A	A	A	
	673-5	1100	A	A	A, S	A	A	A	A	A	A	

[a] Phases listed in decreasing order of intensity.

[b] Code: A, αAl_2O_3; Z, ZrO_2; S, Nickel aluminate spinel, $A_0 = 8.05$ to 8.10 Å; N, NiO.

from 2500 to 3000 hr, even though the specific weight loss was steady throughout the test, as was the speckled metallic appearance of the sample. Even at 1200°C, the amount of collected spall was less than expected. This can be due to a fine powdery spall that was too light to fall completely into the collector cup but was rather dispersed in the air.

Metallography, SEM, and EPMA Results

The microstructures of the three β-NiAl samples after testing at 1200°C are similar in that there is not enough Al depletion at the metal-oxide interface to lead to γ' formation at the metal-oxide interface. The two alloys containing Zr have microstructures with "fingers" protruding into the metal matrix from the external scale. The Zr-free alloy shows no oxide penetration and only a very clean matrix under a thin patchy scale. The scale on the Zr$^-$ containing alloys is thicker and more uniform. The Zr-containing alloys form similar scales at the two other test temperatures. Figure 2 shows the three alloys tested at 1150°C for 3000 1-hr cycles in static air. Alloy 1 shows no oxide penetration and virtually no retained scale. Alloy 2 has a fairly thick, coherent, adherent scale with minor protrusions. Alloy 3 has much deeper scale penetration but with a somewhat thinner, less-coherent surface scale than that of alloy 2.

Thickness changes of the samples before and after test were measured. The Zr-containing alloys have a slight increase in thickness for all of the samples tested. The Zr-free alloy, however, did show a thickness loss of 0.305 mm after 500 hr at 1200°C, and 0.277 mm after 3000 hr at 1150°C. However, the Zr-free alloy at 1100°C after 3000 hr showed the same slight increase in thickness as the Zr-containing alloys.

EPMA was performed on the three alloys after 500 hr at 1200°C. Traces were made for Ni, Al, and Zr. Figure 3a shows the trace for the alloy 1 sample from the metal-oxide interface to 600 μm into the matrix. It shows the steady, linear drop for Al from 28.6 wt.% (46.6 at.%) to 20 wt.% (35.2 at.%). The two Zr-containing alloys 2 and 3 show constant Ni, Al, and Zr concentrations from 600 μm into the matrix until about 50 μm from the metal-oxide interface where the oxide-protruding fingers appear to affect the composition, as shown in Fig. 3b,c.

Figure 4 shows back-scattered electron micrographs of the surface of alloy samples tested at 1150°C for 3000 hr. The light areas indicate the higher atomic-number regions (i.e., base metal). The darker areas indicate regions of lower atomic number (i.e., oxides). This confirms the tendency for the Zr-free alloy 1 to spall to bare metal particularly at the higher temperature. It also shows that alloy 3 apparently spalls to bare metal to some extent, about 5%. After 3000 hr at 1100°C, alloys 1 and 3 both show

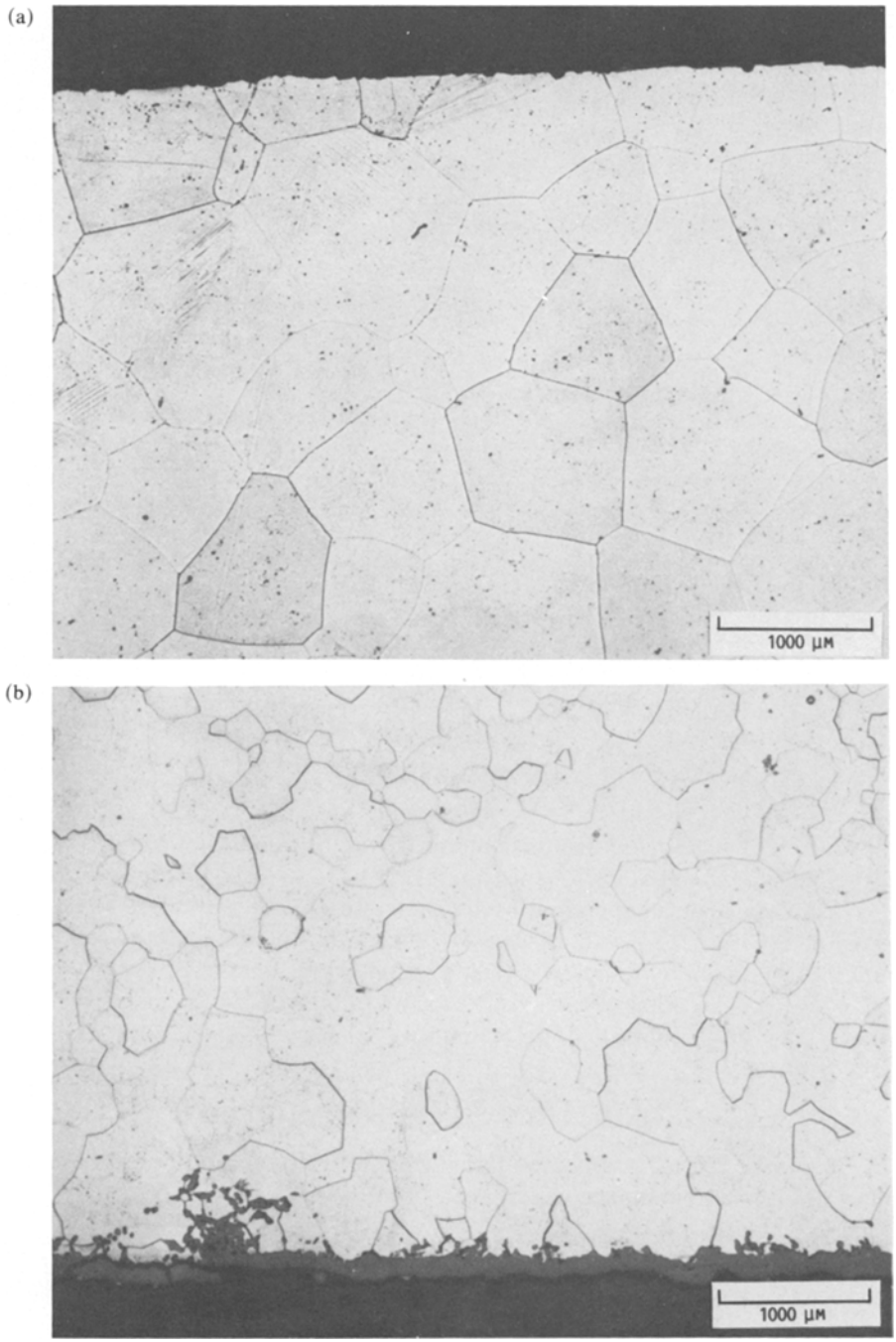

Fig. 2. Post-test microstructures for the three β-NiAl test alloys after 3000 1-hr cycles at 1150°C in static air. (a) Alloy 1 Ni-46.6 at.% Al-O at.% Zr (b) alloy 2 Ni-48.3 at.% Al-0.1 at.% Zr, and (c) alloy 3 Ni-38.1 at.% Al-0.1 at.% Zr.

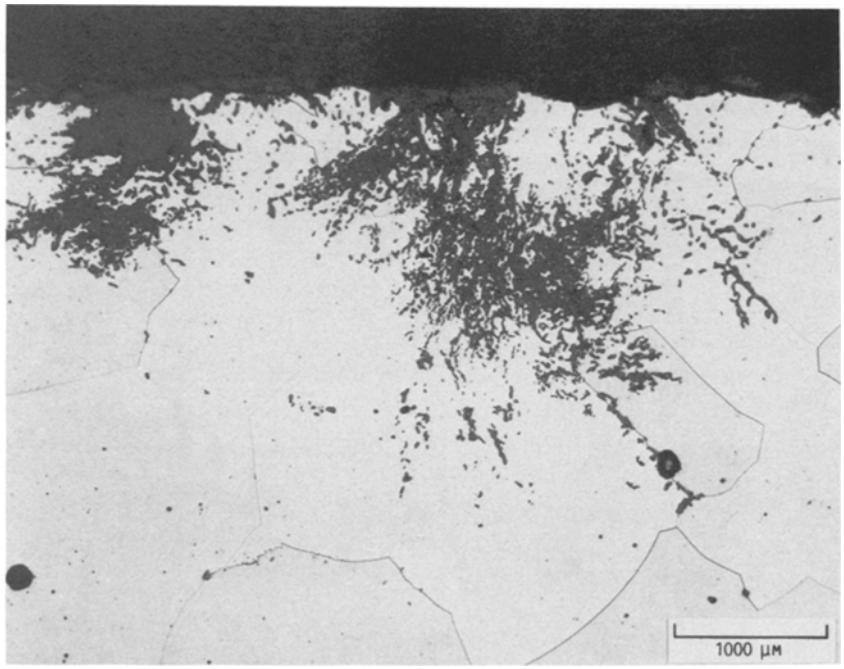

Fig. 2. Continued.

about 1 or 2% bare metal due to spalling. The high-Al alloy with Zr shows negligible bare metal at both temperatures.

Scanning electron micrographs are shown in Fig. 5 for all three alloys tested at 1200°C for 500 1-hr cycles. At 1200°C, alloy 1 again shows some bare metal typified by dimples, crystallographic voids, and imprints of the oxide grains. The other photos tend to show more oxide, particularly in alloy 2 (Fig. 5b), confirming observations by other methods.

CYCLIC OXIDATION COMPUTER MODELING

The three critical gravimetric parameters in the oxidation process are related by the mass balance equation at any time t:

$$\Delta W/A = W_r - W_m \tag{2}$$

where $\Delta W/A$ is the specific weight change values cited previously from experimental data versus time, W_r is the specific weight of oxide formed on the specimen after spalling, and W_m is the specific amount of metal consumed as it is converted to oxide. If any of the scale spalls, the following

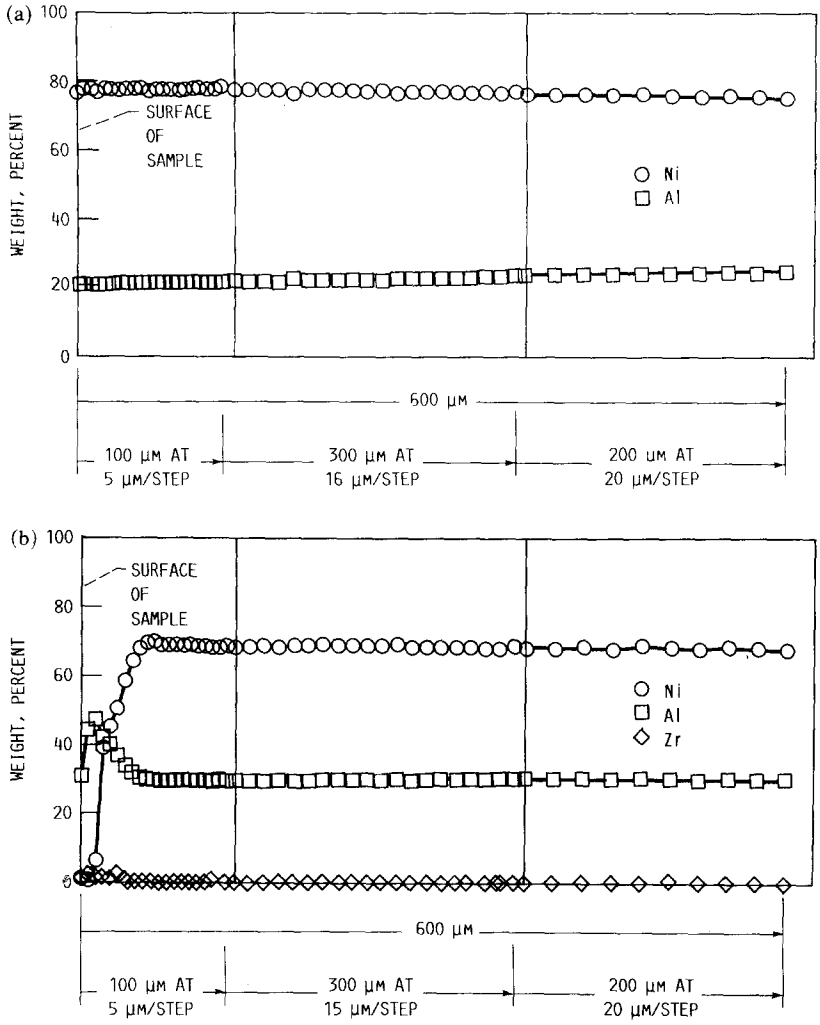

Fig. 3. Electron microprobe traces for Ni, Al, and Zr (where present) for the three β-NiAl test alloys after 500 1-hr cycles at 1200°C in static air. (a) Alloy 1 Ni-46.6 at.%-0 at.%-0 at. % Zr, (b) alloy 2 Ni-48.3 at.% Al-0.1 at.% Zr, and (c) alloy 3 Ni-38.1 at.% Al-0.1 at.% Zr.

expression holds at a given time:

$$W_s = W'_r - W_r \tag{3}$$

where W_s is the specific weight of the oxide spalled and W'_r is the specific weight of the scale at temperature prior to spalling.

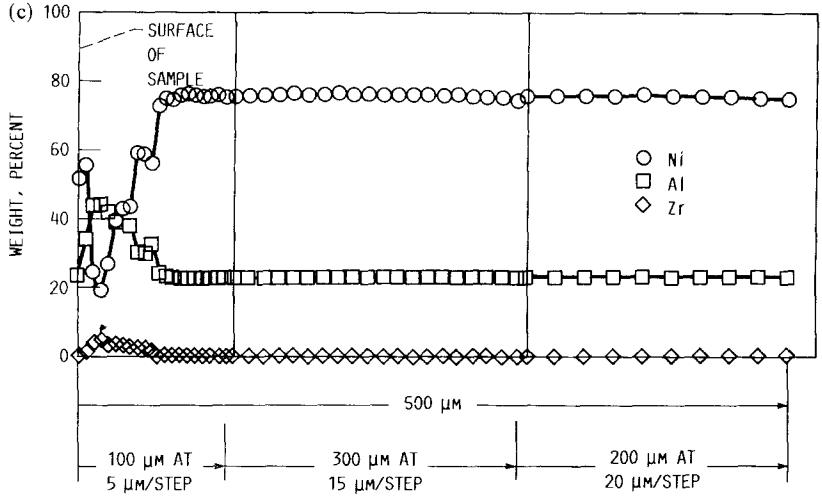

Fig. 3. Continued.

As has been pointed out elsewhere,[11] Eq. (2) can give an excellent fit to the observed specific-weight-change versus time data by regression analysis. However, the derived constants may not be the true rate constants that apply to mechanisms of cyclic oxidation.

The actual cyclic process involves oxidation to form a scale which thickens by diffusional growth. As the sample cools the oxide spalls, thus reducing the oxide thickness, possibly to bare metal. As the sample returns to temperature, growth continues as before but the growth rate is that corresponding to the reduced scale thickness (i.e., the growth rate is increased). In the case of parabolic growth, this is simply a projection back to an earlier part of the growth curve or, in the case of spalling to bare metal, to the beginning of scale growth curve, where its slope (i.e., instantaneous scaling rate) is highest. In the case of the aluminide alloys tested here, the growth rates are parabolic. Therefore, after spalling the rate is assumed to continue to follow the initial or previous growth curve even though the effective time could be considerably less than the actual test time. The remaining problem is to model the spalling process. Equation (2) assumes that the scale spalls at a constant rate after each cycle but actually for spalling

$$W_s = Q_0(W_r')^2 \tag{4}$$

where Q_0 is the probability of spalling. This formulation is based primarily on the work of Lowell.[11] Thus as the scale thickness increases the amount of spall increases. A computer program known as COSP[11,12] was developed

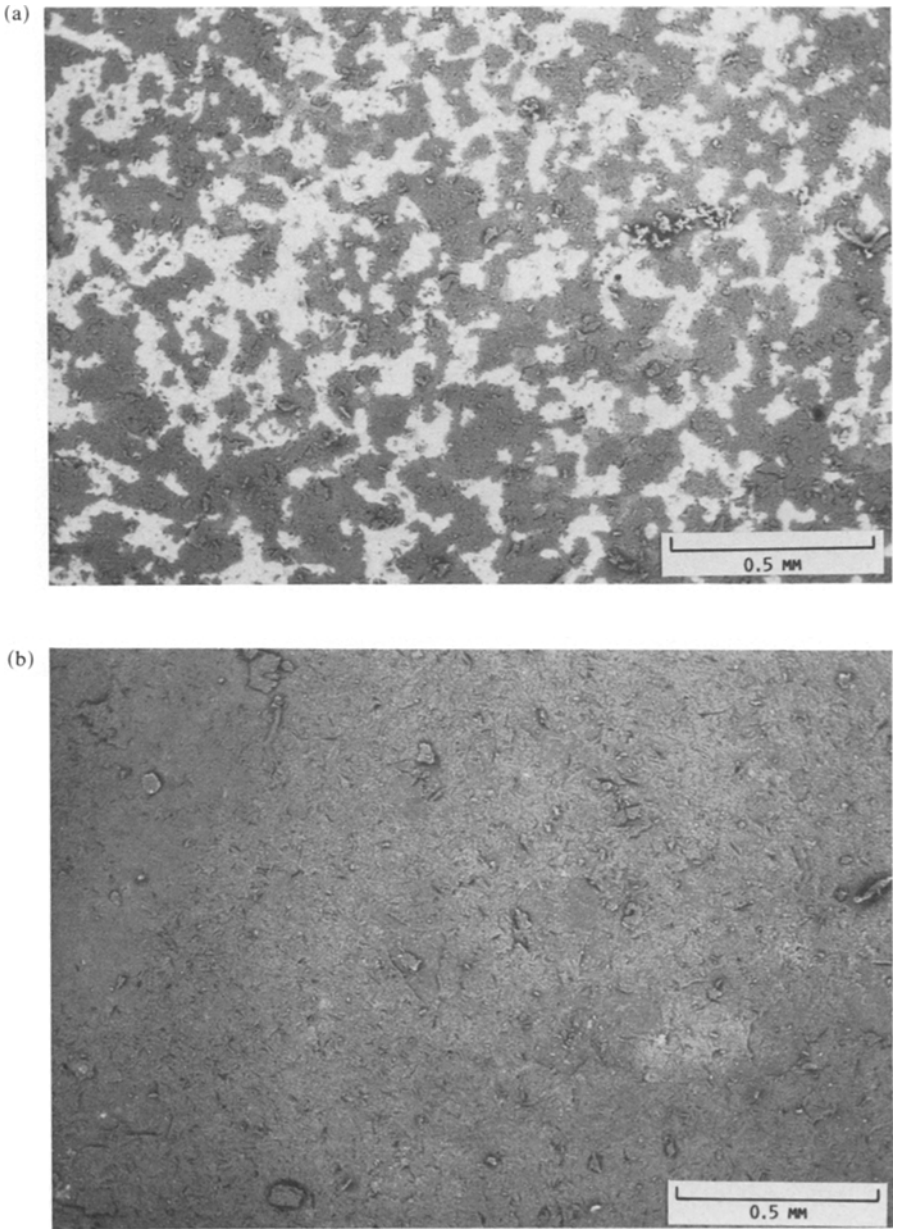

Fig. 4. Back-scattered scanning electron microscopy of the surface of three β-NiAl test alloys after 3000 1-hr cycles at 1150°C in static air. (a) alloy 1 Ni-46.6 at.% Al-0 at.% Zr, (b) alloy 2 Ni-48.3 at.% Al-0.1 at.% Zr, and (c) alloy 3 Ni-0.38.1 at.% Al-0.1 at.% Zr.

(c)

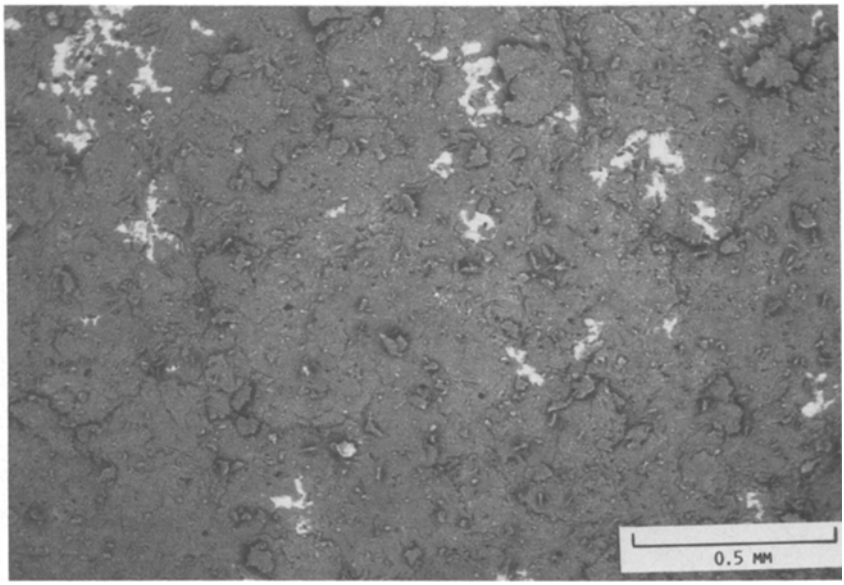

Fig. 4. Continued.

in order to simulate this process for any specified oxide, provided k_p or a scale growth process is known. Q_0 can be measured independently but, because the values for commercial Al_2O_3 formers are generally so low, very large surface areas are required. Although experimentally difficult, ranges of values can be inferred and used in Eq. (4) in COSP to match the experimental gravimetric–time cyclic curves. Special cases of this process occur when spalling to bare metal takes place (i.e., $W_s = W_r'$). In the COSP program, 1 cm^2 is divided into a maximum of 1000 segments. Individual segments are followed for each cycle in which spalling takes place either by spalling to bare metal or by not spalling at all. In the spalling-to-bare-metal case, S_0 is used instead of Q_0 to indicate the spalling probability. In the simplest case, a rectangular distribution is used with a random-number generator. If the random number is normalized, all values below the critical spalling probability S_0 will result in spalling to bare metal; above S_0, no spalling occurs. This process is followed for each segment for each cycle throughout the entire length of the test. This COSP computer program also computes other critical parameters as a function of time, particularly W_m, which is the critical value in any corrosion process, W_r, $\Delta W/A$ crossover times, and so forth.

The COSP program was used cycle by cycle to generate $\Delta W/A$, W_r, and W_m values arising the 100-hr k_p values (or for the Zr-free alloy 1 at

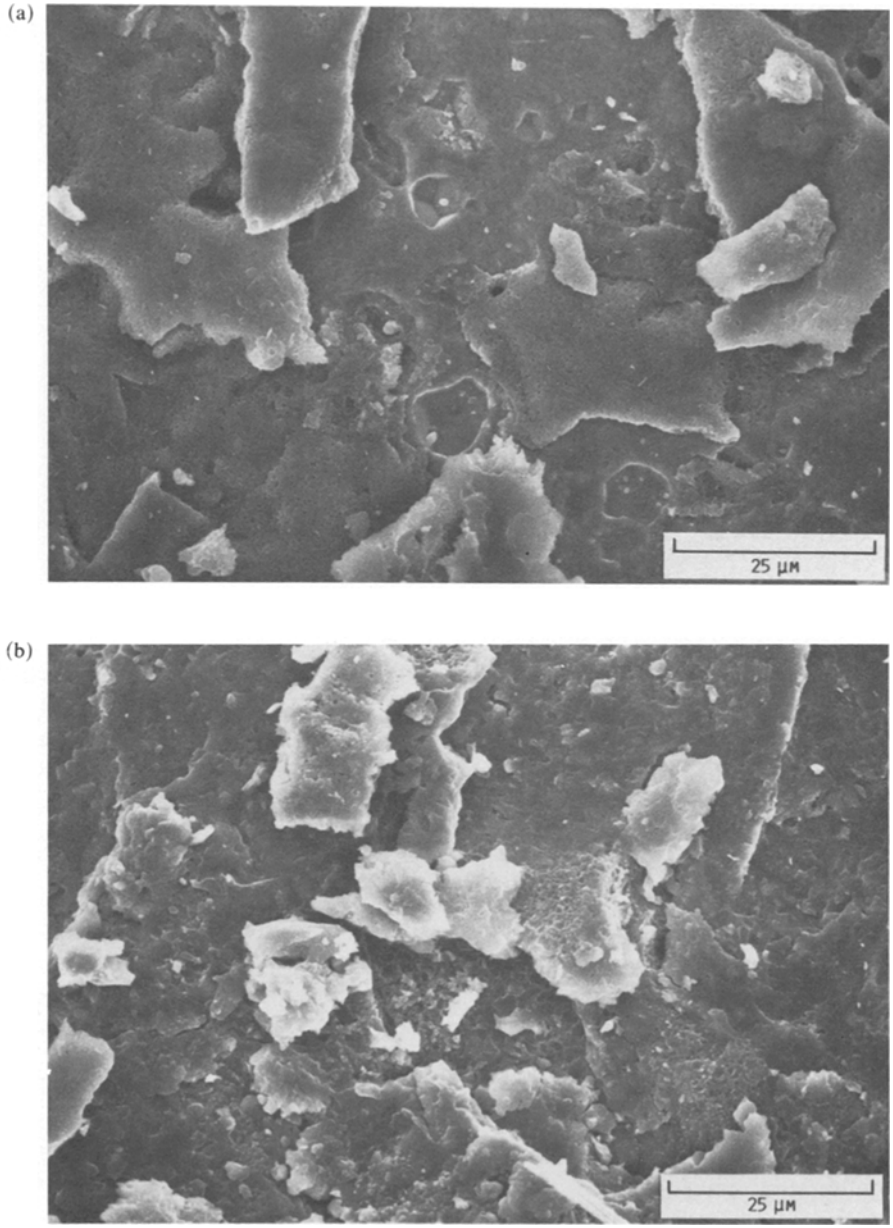

Fig. 5. Detail of surface oxide morphology for three β-NiAl test alloys after 500 1-hr cycles at 1200°C in static air. (a) alloy 1 Ni-46.6 at.% Al-0 at.% Zr, (b) alloy 2 Ni-48.3 at.% Al-0.1 at.% Zr, and (c) alloy 3 Ni-38.1 at.% Al-0.1 at.% Zr.

(c)

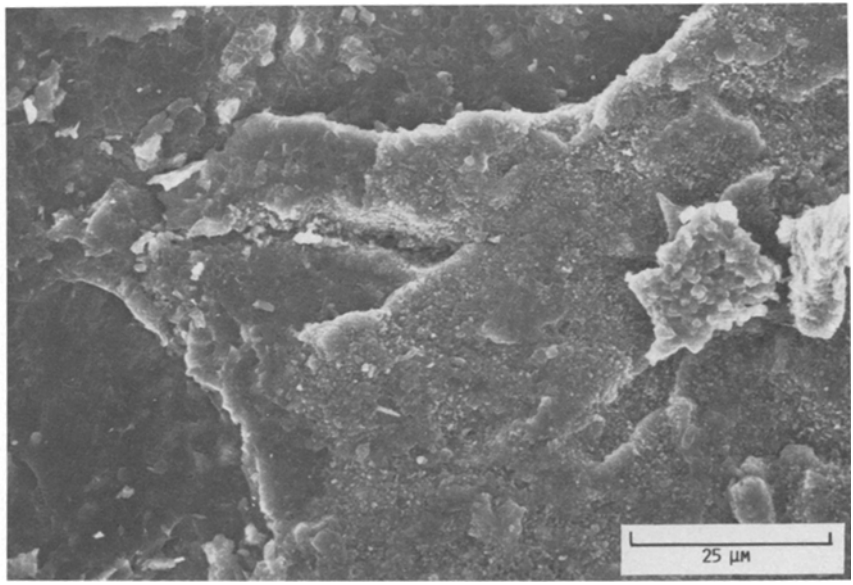

Fig. 5. Continued.

1200 and 1150°C, the isothermal k_p values). Also needed is the stoichiometric constant for the controlling oxide formed on the alloy, designated a_s.* All the $\Delta W/A$-versus-time runs were first fitted to the COSP model following $W_s = (Q_0 W_r')^2$. This gave reasonable fits for alloys 2 and 3 but relatively poorer fits for alloy 1. The fits improved significantly for alloy 1 when the segmented spall to bare metal was used with their corresponding S_0 values.

Table IV summarizes the k_p and derived Q_0 values for each sample of alloys 2 and 3, as well as the S_0 values for alloy 1. The Q_0 and S_0 values are assumed to be constant throughout each test. Also listed as a function of time are the specific weight values W_m of the Al converted to α-Al_2O_3, regardless of whether the oxide spalls. Note that for the Zr-containing alloys even at 1200°C these Q_0 values are extremely low and almost insignificant. This is reflected in the validity of the 100-hr cyclic k_p values.

Some fitted curves for the $\Delta W/A$-versus-time data listed in Table II are compared with the calculated values, from the parameters in Table IV, and are shown in Fig. 6. This set of curves for alloy 2 is typical in that the spalling probability is low with spalling occurring within the scale. Shown in Figs. 7 and 8 are the experimental and calculated curves for the spall-to-bare-metal cases for alloy 1 without Zr at 1200 and 1150°C. Here the degree

*For α-Al_2O_3 $a_s = 1.1242$ derived from $a_s = \dfrac{2 \times \text{at.wt of Al}}{3 \times \text{at. wt. of O}}$.

Table IV. Derived Parameters from COSP Scale Growth/Scale Spalling Computer Simulation Program for β-NiAl Alloy Samples Tested in Cyclic Oxidation from 1100 to 1200°C

Alloy	Run	Temperature, °C	Cycle, hr	Test time, hr	k_p $(mg/cm^2)^2/hr$	S_0[c]	Q_0[d]	W_m, for selected time in hr, mg/cm^2								
								100	200	500	1000	1500	2000	2500	3000	10,000
Ni-46.6Al	660-3	1200	1	500	0.0311[b]	0.25		9.31	18.4	46.0	91.8	138	183	229	275	915
	672-4	1150	1	3000	0.0155[b]	0.015		2.03	3.53	8.12	15.8	23.4	31.1	38.7	46.2	153
	673-4	1100	1	3000	0.000903[a]	0.0021		0.36	0.54	0.98	1.70	2.37	3.06	3.76	4.45	12.8
	673-5	1100	1	3000	0.00139	0.0015		0.44	0.65	1.14	1.91	2.64	3.39	4.11	4.85	13.1
Ni-48.3Al	625-6	1200	1	1000	0.0151[a]		0.000098	1.39	1.97	3.18	4.70	6.06	7.37	8.66	9.94	27.2
-0.1Zr	660-4	1200	1	500	0.0134		0.000051	1.30	1.85	2.95	4.27	5.37	6.40	7.38	8.35	21.6
	672-5	1150	1	3000	0.00662		0.000013	0.91	1.29	2.05	2.91	3.59	4.17	4.70	5.19	10.9
	673-3	1100	1	3000	0.00170		0.000010	0.46	0.66	1.04	1.47	1.81	2.09	2.34	2.58	5.01
	673-6	1100	1	3000	0.00231		0.000020	0.54	0.76	1.21	1.72	2.12	2.46	2.77	3.05	6.34
Ni-38.1Al	660-2	1200	1	500	0.0211[a]		0.000140	1.64	2.34	3.83	5.80	7.65	9.46	11.3	13.1	38.3
-0.1Zr	672-1	1150	1	3000	0.0139		0.000010	1.32	1.87	2.96	4.22	5.13	6.05	6.62	7.54	16.0
	673-2	1100	1	3000	0.00527		~0	0.82	1.15	1.82	2.58	3.16	3.65	4.08	4.47	8.15
	673-2	1100	1	3000	0.00490		~0	0.79	1.11	1.76	2.49	3.05	3.52	3.93	4.31	7.86

[a] k_p derived from 100 hr cyclic data.
[b] k_p derived from 24 hr isothermal data.
[c] S_0-bare metal spall, COSP-model 5, $\alpha = 0$, number segments = 400.
[d] Q_0-fractional scale spall, COSP-model 2, $\alpha = 1$.

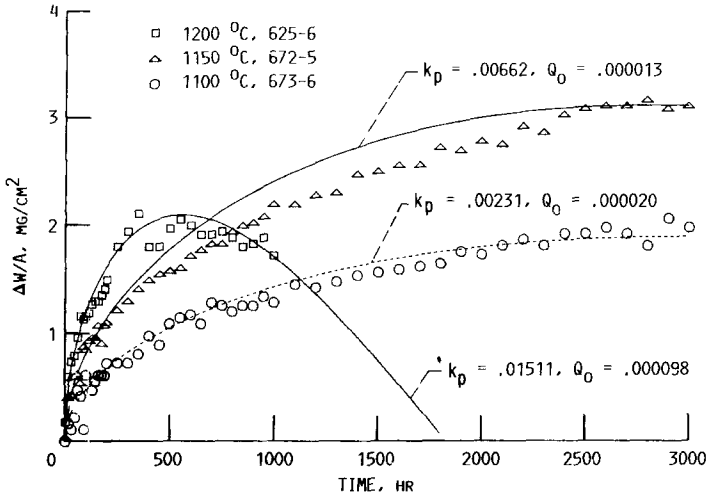
1200 °C, 625-6
1150 °C, 672-5
1100 °C, 673-6
k_p = .00662, Q_0 = .000013
k_p = .00231, Q_0 = .000020
k_p = .01511, Q_0 = .000098
ΔW/A, MG/CM²
TIME, HR
0
500
1000
1500
2000
2500
3000
1
2
3
4

Fig. 6.

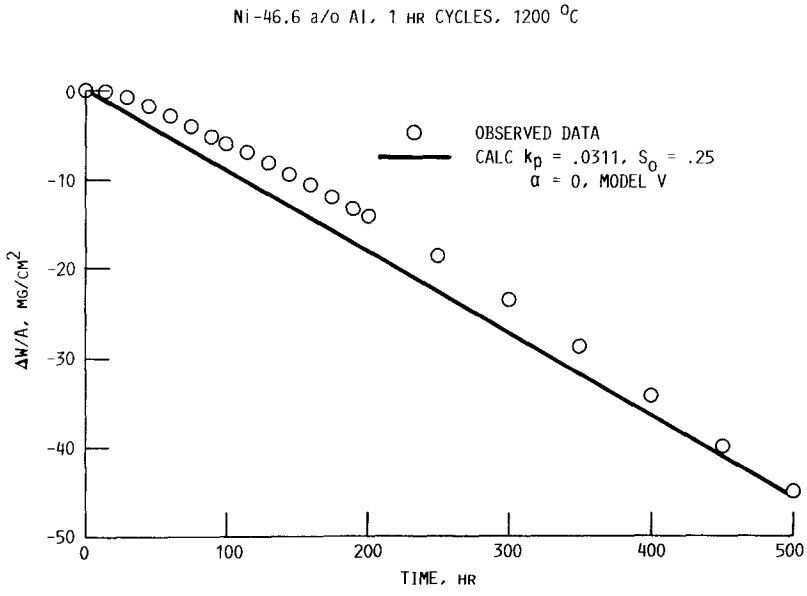
Ni-46.6 a/o Al, 1 HR CYCLES, 1200 °C
OBSERVED DATA
CALC k_p = .0311, S_0 = .25
α = 0, MODEL V
ΔW/A, MG/CM²
TIME, HR
0
-10
-20
-30
-40
-50
0
100
200
300
400
500

Fig. 7.

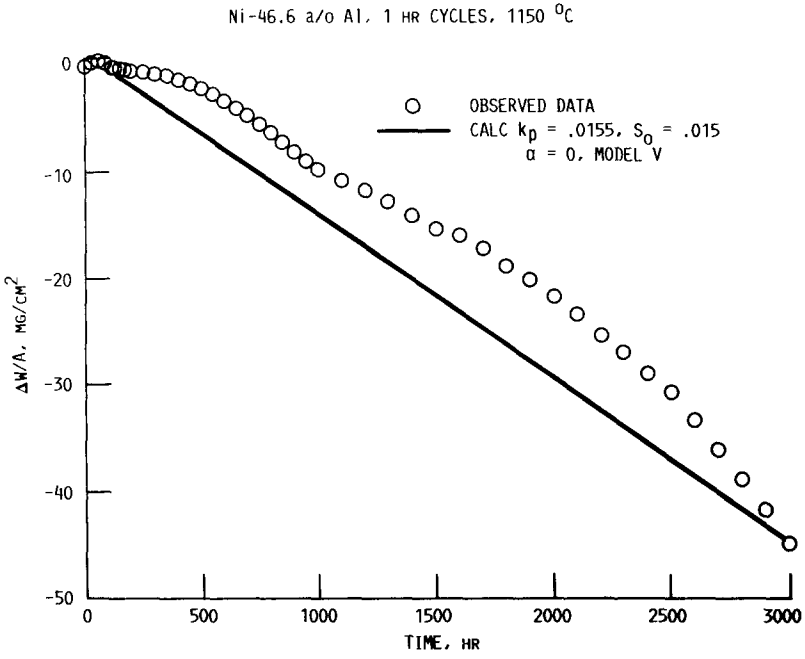

Fig. 8.

of fit is not quite as good as in the spalling-within-the scale case shown in Fig. 6. This implies that the spalling-to-bare-metal model may be more complex (i.e., S_0 may vary with each segment's thickness) or the nature of the oxide might be changing. Some spalling within the scale may be taking place as well. Figure 9 shows the 1100°C data for alloy 1 for the interval of 0–3000 hr for duplicate runs.

A more practical way to interpret the cyclic oxidation results is to consider the effect of cyclic oxidation, with its scale spalling, on the amount of Al actually consumed as it is converted to Al_2O_3. This is the W_m value introduced above. The converted Al is either in the retained scale, designated W_r, or in the spalled oxide W_s. These are specific values—each total divided by the sample area. Figure 10 shows the W_m plots as a function of time on a log-log scale for the alloys at the three test temperatures. In each plot, the straight line at a 30° angle represents parabolic growth of the scale. In this case

$$W_m = a_s(k_p t)^{1/2} \tag{5}$$

where a_s is the stoichiometric constant for Al present in the scale discussed above. The closed symbols in Fig. 10 indicate the same W_m parameter for

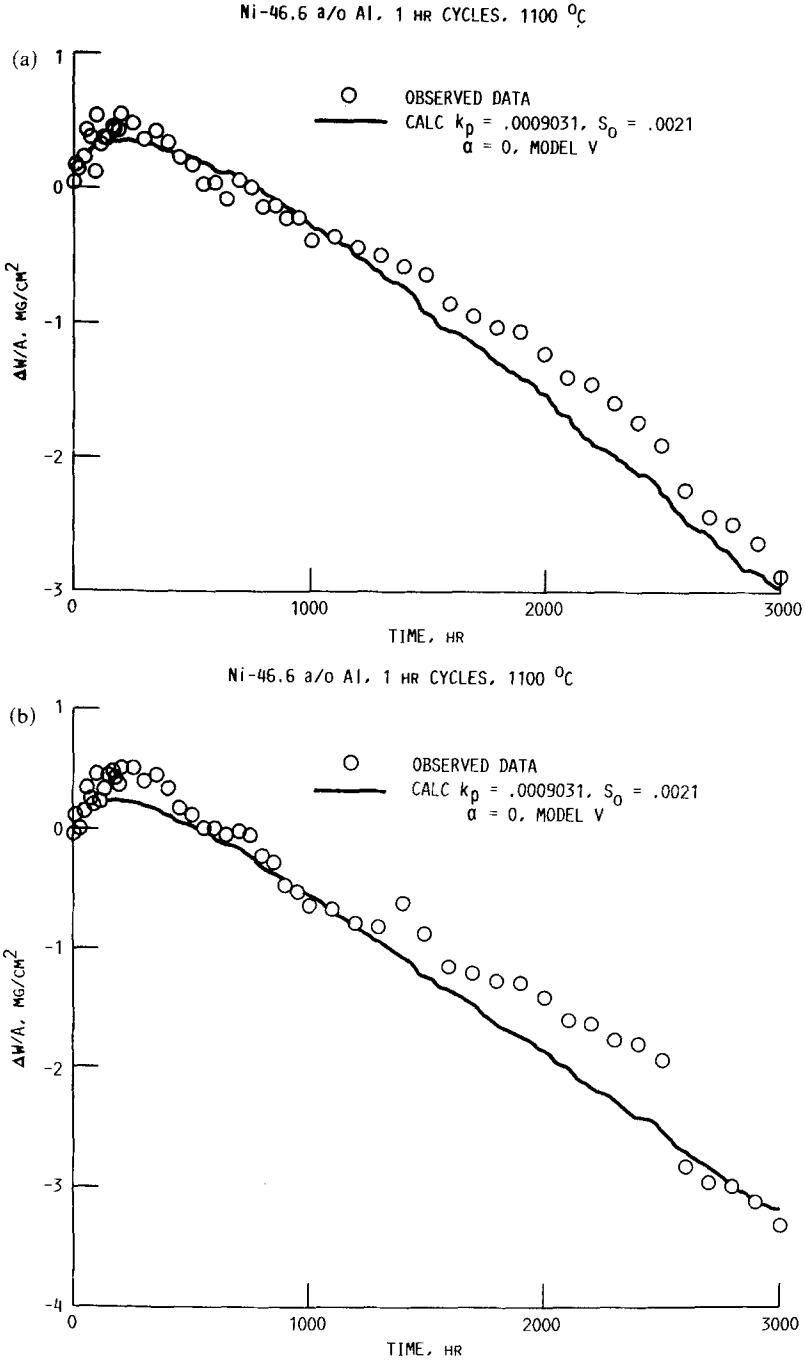

Fig. 9. COSP computer model V fit vector for gravimetric-time data at 1100°C for duplicate samples of the Al_2O_3 scale forming alloy 1 (Ni-46.6 at.% Al-0 at.% Zr) based on the growth and spalling parameters k_p and S_0. (a) sample 673.4. (b) Sample 673.5.

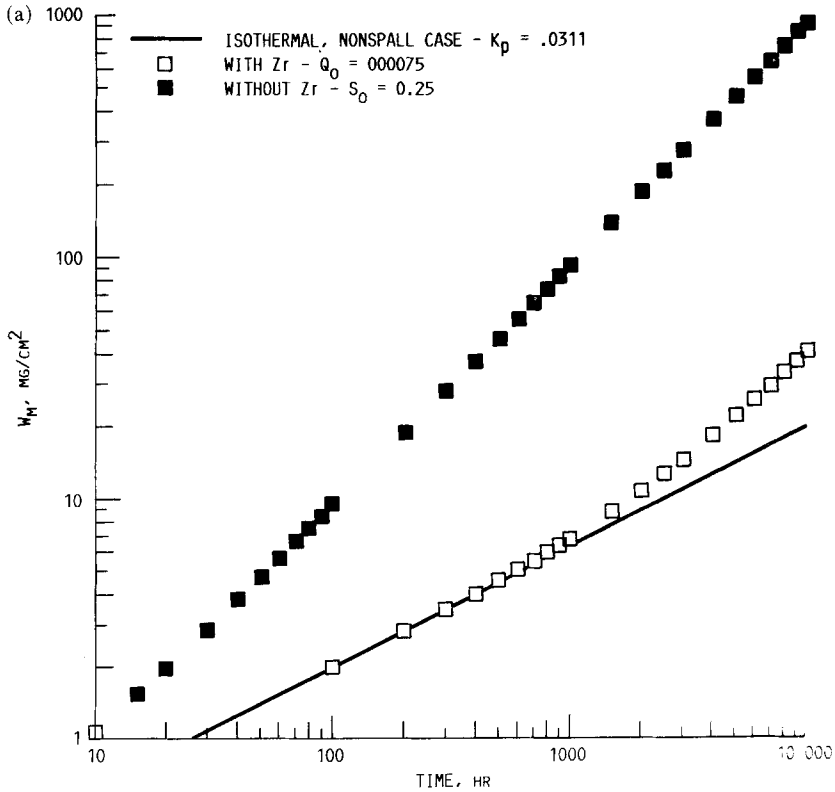

Fig. 10. Comparison of the specific weight of Al consumed, W_m in forming α-Al_2O_3 in 1-hr cyclic oxidation of near-stoichiometric β-NiAl with and without ~0.1 at.% Zr computed out to 10,000 hr at three temperatures in static air. (a) 1200°C. (b) 1150°C. (c) 1100°C.

the case of the spalling-to-bare-metal model with spalling probabilities, $S_0 = 0.25$ for 1200°C, $S_0 = 0.015$ at 1150°C, and $S_0 = 0.0015$ at 1100°C, respectively. For the first two cases, the W_m values increase rapidly with time. The open symbols in Fig. 10 represent the effect when 0.10 at.% Zr (~0.18 wt.%) is added to the alloy, leading to a low probability of within-scaling spalling. At 1200°C, the W_m values are virtually identical to those of the simple parabolic case results for the Zr-containing samples, until some slight divergence starting near 1000 hr. For the Zr-free alloy, a specific metal consumption of 10 mg/cm^2 is obtained at 100 hr. For the Zr-containing alloy, a 10 mg/cm^2 W_m is not reached until after 1500 hr. At 1150°C, the curve for the Zr-containing alloy does not diverge significantly from the parabolic curve until after 3000 hr. For the Zr-free alloy, a 10 mg/cm^2 W_m is reached at approximately 600 hr, while this value is reached in the

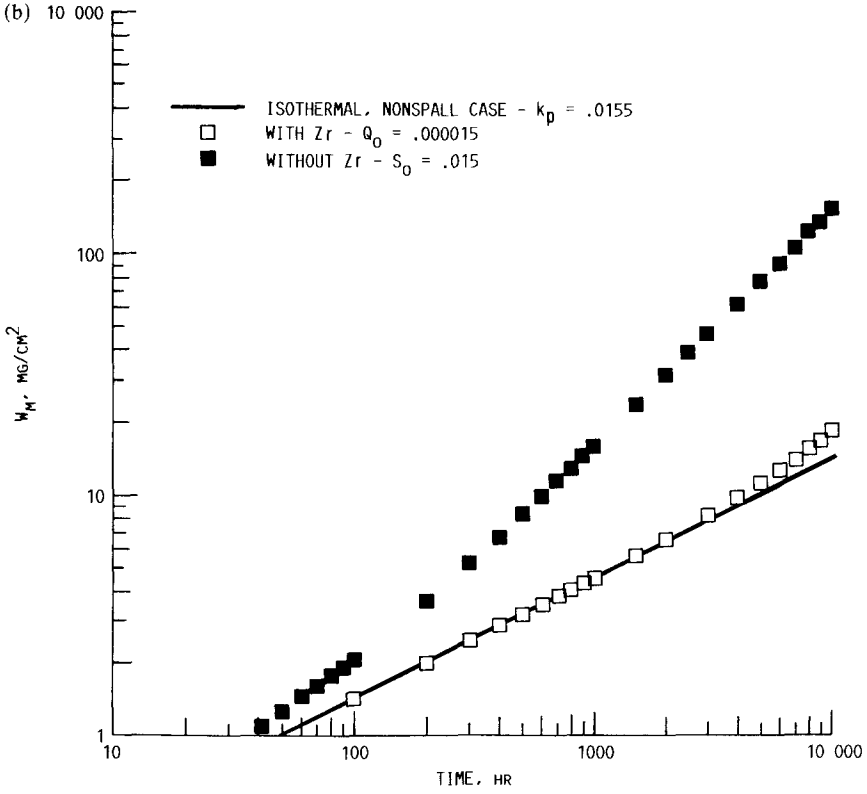

Fig. 10. Continued.

−0.1 at.% Zr alloy near 4500 hr. At 1100°C, a value of 10 mg/cm^2 for W_m is reached at ~7000 hr for the Zr-free β-NiAl, while the Zr addition raises the 10 mg/cm^2 W_m value well beyond 10,000 hr. The Zr is still beneficial, but the effect is much smaller.

Metallography and SEM of the three alloy samples also show the distinct difference between the Zr-free alloy that spalls to bare metal and the two Zr-containing alloys that spall lightly within the scale. By using the mass balance, Eq. (4) and solving for W_r at 500 hr for the 1200°C runs, the specific weight (i.e., thickness) of the Zr-free alloy scale is roughly 1/10 that for the Zr-containing alloys. Figures 7-9 for the three alloys at 1150°C for 3000, 1-hr cycles show the much thicker oxide retained on the two alloys with Zr. They also show that the scales tend to penetrate well into the alloy which may help in anchoring it, minimizing spalling. The SEM photos for the same alloys show the same spall-to-bare-metal or within-scale spalling effects.

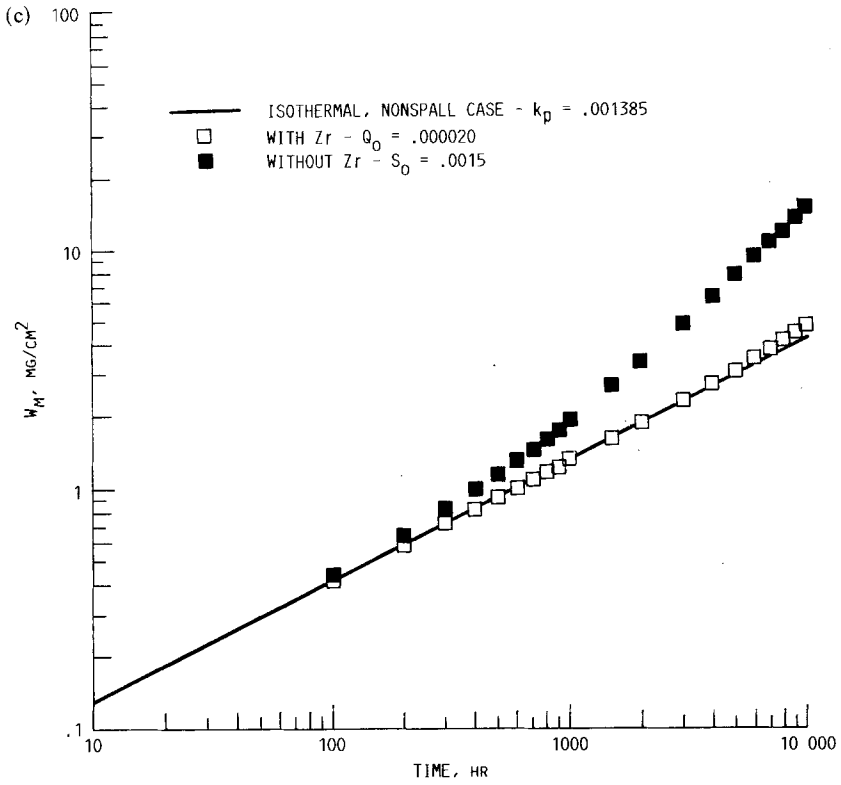

Fig. 10. Continued.

A possible reason why the Zr-free alloy spalls so drastically to bare metal has been suggested by Smeggil.[13] It is supposedly due to residual sulfur levels in the alloy that alter the scale adhesion at the metal-oxide interface by "poisoning" the surface. Smialek[14] investigated the gettering effect of Zr in NiCrAl alloys and determined that for "low" sulfur levels (<500 ppm) a Zr level of greater than $600 \cdot (\mathrm{Su})^{0.2}$, where Su is the sulfur content in atomic ppm, is needed. However, sulfur levels of the three hipped alloys tested herein were found to be below the detection limit of 10 ppm for nickel-base alloys. Therefore Smeggil's sulfur-poisoning thesis remains unproved for these alloys.

At 1100°C, however, there appears to be only a slight difference in the cyclic oxidation behavior of the three β-NiAl alloys at least based on gravimetric results. For example, as can be seen from Table V, the W_m values at 1000 hr are close to a value of 2 mg/cm^2 for all three alloys. At 3000 hr, the W_m values are 3–4 mg for all three alloys. Therefore, a low Zr

Table V. Derived Parabolic Scaling Constants, k_p, for Various β-Nickel Aluminide Alloy Samples for this and Other Investigations (Temperature range 1273 to 1563 K)

	Al, at.%	Temperature, °K	Trace additions	k_p	Method of determining k_p	Reference[b]
1	48.3	1473	Zr-0.1 at.%	0.01511	Gravimetric-from 100 hr cyclic data	—
2	48.3	1473	Zr-0.1 at.%	0.01338	Gravimetric-from 100 hr cyclic data	—
3	48.3	1473	Zr-0.1 at.%	0.02676	Gravimetric-from 24 hr isothermal data with Cahn microbalance	—
4	48.3	1423	Zr-0.1 at.%	0.006619	Gravimetric-from 100 hr cyclic data	—
5	48.3	1423	Zr-0.1 at.%	0.01411	Gravimetric-from 24 hr isothermal data with Cahn microbalance	—
6	48.3	1373	Zr-0.1 at.%	0.001703	Gravimetric-from 100 hr cyclic data	—
7	48.3	1373	Zr-0.1 at.%	0.002310	Gravimetric-from 100 hr cyclic data	—
8	38.1	1473	Zr-0.1 at.%	0.02115	Gravimetric-from 100 hr cyclic data	—
9	38.1	1423	Zr-0.1 at.%	0.01388	Gravimetric-from 100 hr cyclic data	—
10	38.1	1373	Zr-0.1 at.%	0.005275	Gravimetric-from 100 hr cyclic data	—
11	38.1	1373	Zr-0.1 at.%	0.004900	Gravimetric-from 100 hr cyclic data	—
12	46.6	1473	0	0.0311	Gravimetric-from 24 hr isothermal data with Cahn microbalance	—
13	46.6	1423	0	0.0155	Gravimetric-from 24 hr isothermal data with Cahn microbalance	—

14	46.6	1373	0	0.0009031	Gravimetric-from 100 hr cyclic data	—
15	46.6	1373	0	0.001385	Gravimetric-from 100 hr cyclic data	—
16	50.8	1573	0	0.1550	SEM scale thickness as a function of the time—18 days	17
17	50.8	1473	0	0.06994	SEM scale thickness as a function of the time—16 days	17
18	42.0	1573	0	0.06475	Gravimetric-from 16 hr isothermal data with Ainsworth microbalance	16
19	42.0	1473	0	0.02122	Gravimetric-from 20 hr isothermal data with Ainsworth microbalance	16
20	42.0	1373	0	0.001637	Gravimetric-from 20 hr isothermal data with Ainsworth microbalance	16
21	42.0	1273	0	0.000259	Gravimetric-from 20 hr isothermal data with Ainsworth microbalance	16
22	48.7	1373	0	0.003273	SEM scale thickness as a function of time—360 hr	15
23	48.7	1373	Y implant	0.001438	SEM scale thickness as a function of time—360 hr	15
24	41.8	1373	0	0.00298	Gravimetric-cyclic data paralinear curve spall model—1000 hr[a]	4
25	41.8	1373	0	0.00258	Gravimetric-cyclic data paralinear curve spall model—1000 hr[a]	4
26	41.8	1373	0	0.00270	Gravimetric-from 200 hr isothermal data	4
27	41.8	1373	0	0.00300	SEM scale thickness as a function of time—1500 hr	4
28	47.2	1373	Zr-0.05 at.%	0.00461	Gravimetric from 100 hr isothermal data with Cahn microbalance	10

[a] Paralinear curve fit $k_p + k_s$ (spall probability)—Fig. 11 (Ref. 4).
[b] Dashes indicate data from this investigation.

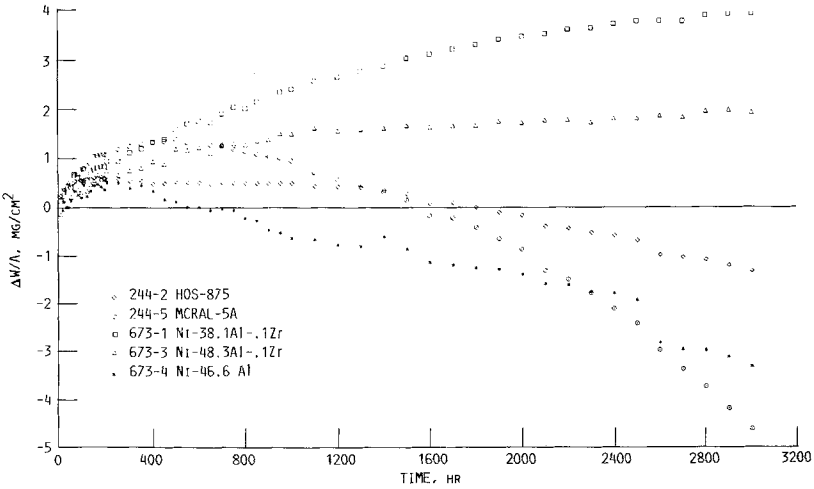

Fig. 11.

addition of ~0.20 wt.% seems to guarantee excellent cyclic oxidation resistance for any practical usage time. The nature of the spalling has not changed for the Zr-free alloy, but bare-metal spalling is much less severe at this lower temperature.

Figure 11 shows the $\Delta W/A$-versus-time plots at 1100°C for 1-hr cycles out to 3000 hr for the three β-NiAl alloys as well as two other alloys tested at this laboratory. They are the iron-base FeCrAl heater alloy, HOS-875, and a NiCrAl(Zr) coating alloy, 5A, developed at this laboratory. These two additional alloys were also analyzed with the COSP program after deriving k_p values from the earlier time-cyclic data. These two alloys also were α-Al_2O_3 formers and followed the spall-within-scale model as well. HOS-875 had a k_p value of 0.00482 and Q_0 of 0.00173, and alloy 5A had a k_p value of 0.12079 and a Q_0 value of 0.000138. These gave W_m values at 3000 hr of 5.09 mg/cm^2 for HOS-875 and 9.29 for alloy 5A. This shows the superiority of the β-NiAl alloys as potential coatings at 1100°C. This is even more pronounced at 1150 and 1200°C, if the β-NiAl alloy contains the small amount of Zr.

COMPARISON WITH OTHER INVESTIGATIONS

In the literature, there are only a limited number of studies on the oxidation behavior of β-NiAl, most of which are isothermal. A comparison can be made by contrasting the k_p values at temperatures from 1000°C to 1300°C, as shown in Table V for the various alloys reported in the literature

tested with a range of Al levels in the β-regime.[4,10,15-17] These values are also plotted in Fig. 12 on a standard Arrhenius plot. Although the Al content, the methods of preparation of the alloys, and the techniques of measuring scale growth vary, the agreement appears good. Included are two k_p estimates for alloys, which also had small amounts of third-element additions.

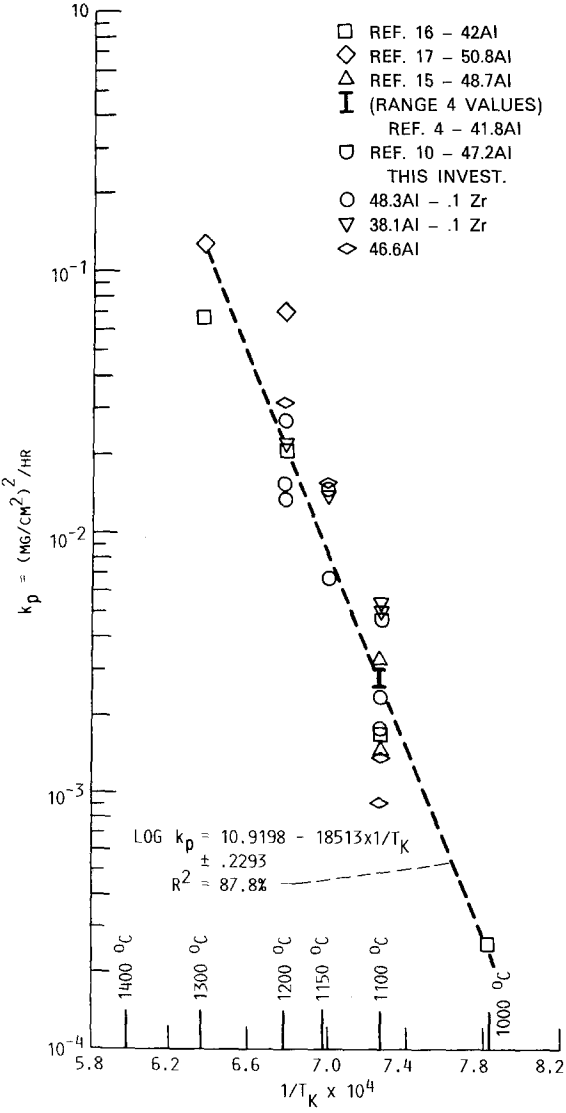

Fig. 12.

One was for a Y-implanted sample[15]; another had a Zr level slightly lower than those investigated here.[10] In general, they fall within the range of k_p values of those tested here.

The 28 k_p values derived for the β-NiAl alloys were fitted by multiple linear regression as a function of $1/T$ and Al content and with a dummy variable if the alloy contained either Zr or Y, or both, in any form. $1/T$ was the only variable that was significant, giving an overall R^2 (in regression the ratio of explained to total variability) value of close to 88%. The coefficient of −18513 gives an estimated activation energy of 84,710 cal/mole.

Two other studies on the cyclic oxidation resistance β-NiAl have been conducted at this laboratory.[2-4] In 1971 and 1972, Lowell and Santoro studied third-element additions of Si, Cr, or Ti effects on the cyclic oxidation resistance to β-NiAl using a series of induction-melted alloys based on Ni-50 at.% Al. The results are summarized in Table VI based on specific weight loss after 200 1-hr cycles in static air at 1200°C. Also included are the two most oxidation-resistant of those alloys retested as part of this investigation, along with the alloys reported herein. The thickness-change recession values, where available, are listed as well. The results indicate that Si is not a beneficial additive, and Cr actually appears detrimental. Ti

Table VI. Comparison of Thickness Change after 1200°C Cyclic Oxidation Testing for Several Times for Various β-Nickel Aluminide Alloys

Alloy, at.%	Test, time/hr	Run[e] (reference)[2]	$\Delta W/A$ Values at 200 1-hr cycle	Recession 1-side-μm
Ni-50.5Al	200	2	−3.83	20.0
Ni-48.8Al-1.1Cr	90	2	−3.73[a]	23.8[b]
Ni-47.6Al-2.6Cr	100	2	−16.02[b]	64.0[b]
Ni-48.8Al-1.1Si	200	2	−3.96	25.9
Ni-46.8Al-2.9Si	200	2	−4.23	22.2
Ni-49.6Al-1.11i	200	2	−2.38	11.5
Ni-47.6Al-3.11i	200	2	+3.19[c]	6.5
Ni-49.6Al-1.11i (410-3)	200	—	−1.50	Slight+
Ni-47.6Al-3.11i (410-1)	200	—	−3.55	89.0
Ni-46.6Al (660-3)	500	—	−14.06	152.5[d]
Ni-48.3Al-0.1Zr (625-6)	1000	—	1.48	—
Ni-48.3Al-0.1Zr (660-4)	500	—	1.62	Not
Ni-38.1Al-0.1Zr (660-2)	500	—	2.01	sig.

[a] Value(s) at 90 hr.
[b] Value(s) at 100 hr.
[c] Possible cracks.
[d] Value(s) at 500 hr.
[e] Dashes indicate this investigation.

does offer some improvement in cyclic oxidation resistance, but not to the degree that much smaller amounts of Zr do. *H*f would probably be beneficial as well. Smialek at this laboratory tested a Ni-42 at.% Al alloy at 1100°C for various cycle times (1, 20, and 50 hr) for times to 500 hr. The alloy contained no Zr. The specific weight-change-versus-time data were analyzed using parabolic scaling growth with the spalling-to-bare-metal model but with simplified assumptions, because at that time the COSP computer program was not yet available. His k_p values (listed in Table VI, inferred from the spall model), measured isothermally and derived from scale thickness, were in good agreement. The derived S_0 values of 0.0021 and 0.0016 at 1100°C for 3000 1-hr cycles for the two Ni-46.6 Al samples are close to Smialek's k_s values of 0.0012 and 0.0016. This lends credence to the conclusion that the major mode of oxide spalling in Zr-free β-Ni aluminide is spalling at the metal-oxide interface (i.e., bare-metal spalling).

SUMMARY OF RESULTS

Three hipped β-NiAl alloys: Ni-46.6 at.% Al, Ni-48.3 at.% Al-0.1 at.% Zr, and Ni-38.1 at.% Al-0.1 at.% Zr, were tested in cyclic oxidation in static air at 1100, 1150, and 1200°C. One-hour exposure cycles were used for test times up to 3000 hr. Specific weight-change-versus-time data along with XRD, SEM, microprobe and metallographic analyses were used to evaluate the results. For detailed analysis each gravimetric run was modeled by the computer program COSP to gain further insight into the cyclic oxidation process as well as to predict W_m, the specific metal consumption. The conclusions can be summarized as follows:

1. Small amounts of Zr (~0.1 at.%) alloyed with β-NiAl dramatically increased the cyclic oxidation resistance of the alloy by minimizing α-Al_2O_3 spalling during the cooling cycles.
2. The scale-spall resistance is associated with small amounts of ZrO_2 in the α-Al_2O_3 scale.
3. Without the Zr, the oxide spalls randomly at the metal-oxide interface (i.e., to bare metal) ranging from 25% of the surface area per cycle at 1200°C to ~0.2% of the area at 1100°C. The spall occurs as very fine particles.
4. With ~0.1 at.% Zr in the alloy, the scale spalls within the oxide only to ~0.1% or less of its total thickness or less per cycle at 1200°C to ≤0.001% at 1100°C.
5. In terms of estimates of specific metal consumed, W_m (i.e., Al in the alloy converted to Al_2O_3, retained or spalled) a value of 10 mg/cm^2 is reached for the Zr-free β-NiAl after nearly 110 hr at 1200°C, whereas the Zr addition to the near-stoichiometric alloy

increases the time to reach this same W_m value to 2500 hr. By contrast at 1100°C, the 10-mg/cm^2 level is reached after ~6600 hr for the Zr-free alloy. The comparable alloy with Zr achieves this level at approximately 60,000 hr.

6. Diffusion gradients derived from microprobe analyses indicate a steady, linear, Al-loss gradient from the center of the surface of the sample for the Zr-free alloy, particularly at 1150°C and 1200°C. The Al gradients for the Zr-containing aluminides show minimal Al surface depletion for any of the conditions tested.
7. Photomicrographs indicate that the α-Al_2O_3 scale retained on the Zr-free β-NiAl is patchy and much thinner than the α-Al_2O_3 scale formed on the aluminides with Zr.
8. At 1150°C and 1200°C, the higher, Al-containing β-NiAl with Zr appears to have better cyclic oxidation resistance. At 1100°C, the attack for the three alloys is so low that there is no significant difference in tests performed to 3000 cycles.
9. The mechanism of improved scale adhesion imparted by the Zr to the α-Al_2O_3 is not well understood. Of the possible mechanisms, Zr gettering of sulfur to minimize sulfur poisoning at the metal-oxide interface seems the most reasonable. But sulfur levels were below the 10-ppm detection level for Ni-base alloys.

REFERENCES

1. W. A. Sanders and C. A. Barrett, NASA TN D-6400, July 1971.
2. C. E. Lowell and G. J. Santoro, NASA TN D-6838, 1972.
3. J. L. Smialek and C. E. Lowell, *J. Electrochem. Soc.* **121**, 800 (1974).
4. J. L. Smialek, *Metall. Trans. A* **9A**, 309 (1978).
5. I. Zaplatynsky, NASA TM-87173, 1985.
6. I. Zaplatynsky and C. A. Barrett, NASA TM-88840, 1986.
7. C. A. Barrett and C. E. Lowell, *Oxid. Met.* **11**, 199 (1977).
8. C. A. Barrett and C. E. Lowell, *Oxid. Met.* **12**, 293 (1978).
9. C. A. Barrett, A. S. Khan, and C. E. Lowell, *J. Electrochem. Soc.* **128**, 25 (1981).
10. J. K. Doychak, NASA Contractor Report 175097, 1986.
11. C. E. Lowell, J. L. Smialek, and C. A. Barrett, *High Temperature Corrosion, NACE-6* (1983), pp. 219-226.
12. C. E. Lowell, C. A. Barrett, R. W. Palmer, and J. L. Smialek, COSP—A Computer Program to Model Cyclic Oxidation (in preparation).
13. J. G. Smeggil, *Mater. Sci. Engr.* **87**, 261 (1987).
14. J. L. Smialek, NASA TM-100209, 1987.
15. K. Przybylski and S. Mrowec, *Proceedings Compte Renodu, Vol. 1*, Toronto, June 3-7, 1984.
16. F. S. Pettit, *Trans. AIME* **239**, 1296 (1967).
17. H. M. Hindam and W. W. Smeltzer, *J. Electrochem. Soc.* **127**, 1630 (1980).